





Quantum disordered state in the J_1 - J_2 square-lattice antiferromagnet $\text{Sr}_2\text{Cu}(\text{Te}_{0.95}\text{W}_{0.05})\text{O}_6$

Sungwon Yoon ^{1,2} Wonjun Lee,¹ S. Lee,^{1,3} J. Park,¹ C. H. Lee,¹ Y. S. Choi,¹ S.-H. Do,^{1,4} Woo-Jae Choi,⁵ Wei-Tin Chen,^{6,7} Fangcheng Chou,^{6,7,8} D. I. Gorbunov,⁹ Yugo Oshima ¹⁰ Anzar Ali ¹¹ Yogesh Singh,¹¹ Adam Berlie,³ I. Watanabe ¹² and Kwang-Yong Choi^{1,13,*}

¹Department of Physics, Chung-Ang University, Seoul 06974, Republic of Korea

²TRIUMF, 4004 Wesbrook Mall, Vancouver, B.C., Canada V6T 2A3

³ISIS Neutron and Muon Source, Science and Technology Facilities Council, Rutherford Appleton Laboratory, Didcot OX11 0QX, United Kingdom

⁴Max Planck POSTECH/Hsinchu Center for Complex Phase Materials, POSTECH, Pohang 37673, Republic of Korea

⁵Department of Emerging Materials Science, DGIST, Daegu 42988, Republic of Korea

⁶Center for Condensed Matter Sciences, National Taiwan University, Taipei 10617, Taiwan, Republic of China

⁷Taiwan Consortium of Emergent Crystalline Materials, Ministry of Science and Technology, Taipei 10622, Taiwan, Republic of China

⁸National Synchrotron Radiation Research Center, Hsinchu 30076, Taiwan, Republic of China

⁹Dresden High Magnetic Field Laboratory (HLD-EMFL), Helmholtz-Zentrum Dresden-Rossendorf, Dresden D-01328, Germany

¹⁰Condensed Molecular Materials Laboratory, RIKEN Cluster for Pioneering Research, Hirosawa 2-1, Wako, Saitama 351-0198, Japan

¹¹Department of Physical Sciences, Indian Institute of Science Education and Research Mohali, Sector 81, S. A. S. Nagar, Manauli 140306, India

¹²Meson Science Laboratory, Nishina Center, RIKEN, 2-1 Hirosawa, Wako, Saitama 351-0198, Japan

¹³Department of Physics, Sungkyunkwan University, Suwon 16419, Korea



(Received 16 August 2020; revised 22 November 2020; accepted 24 December 2020; published 21 January 2021)

The B -site ordered double perovskites $\text{Sr}_2\text{Cu}(\text{Te}_{1-x}\text{W}_x)\text{O}_6$ provide an excellent arena for investigating exotic phases expected for the J_1 - J_2 square-lattice Heisenberg antiferromagnet. Here, combining magnetic susceptibility and specific-heat measurements with electron spin resonance (ESR) and muon spin rotation/relaxation (μSR) techniques, we explore a spin-liquid-like state in the vicinity of the Néel critical end point ($x = 0.05$ – 0.1). The specific heat and the ESR and muon relaxation rates give evidence for an energy hierarchy of low-energy excitations, reminiscent of randomness-induced singlet states. In addition, the weak transverse μSR data show a fraction of frozen magnetic moments in the random-singlet background. The origin of a random-singlet-like state near the phase boundary is discussed in terms of concomitant exchange randomness and local strain generated by the W^{6+} -for- Te^{6+} substitution.

DOI: [10.1103/PhysRevMaterials.5.014411](https://doi.org/10.1103/PhysRevMaterials.5.014411)

I. INTRODUCTION

Exchange randomness or quenched disorders have been recently proposed as an efficient route to achieve novel states of matter, including quantum spin liquids (QSLs), valence-bond glass, and random-singlet states. The randomness-induced QSLs become stabilized as long as the moderate randomness is introduced to frustrated magnets irrespective of their spatial dimensionality, type of exchange interactions (Heisenberg and Kitaev), and lattice geometry (triangular, Kagome, honeycomb, and square lattices) [1–9]. In this vein, the $s = 1/2$ J_1 - J_2 square-lattice Heisenberg antiferromagnets (SLHAFs) constitute an excellent platform to delve into randomness-induced exotic states as the competing nearest-neighbor J_1 (a side of the square) and next-nearest-neighbor J_2 (a diagonal of the square) interactions can be continuously tuned in certain systems.

Motivated by Anderson's proposal [10], there have been long-standing endeavors to search a QSL state in the maximally frustrated regime ($|J_2/J_1| = 0.5$) of the $s = 1/2$ J_1 - J_2 SLHAF model [11–14]. It is well-established that in the J_1 dominant regime ($|J_2/J_1| \lesssim 0.4$) Néel order is stabilized, while in the J_2 dominant side ($|J_2/J_1| \gtrsim 0.6$) collinear antiferromagnetic order occurs. In the intermediate regime ($|J_2/J_1| \simeq 0.4$ – 0.6), numerical studies provide cumulative evidence for a QSL state. Until now, a dozen $s = 1/2$ J_1 - J_2 SLHAF candidate materials have been known [15,16,18], yet the putative QSL phase remains uncharted due to the lack of relevant materials.

The B -site ordered double perovskites $\text{Sr}_2\text{Cu}(\text{Te}_{1-x}\text{W}_x)\text{O}_6$ are the recent addition to a class of the $s = 1/2$ J_1 - J_2 SLHAFs [see Fig. 1(a) for its crystal structure] [16–18]. Thanks to the similar size of the Te^{6+} and W^{6+} ions, $\text{Sr}_2\text{Cu}(\text{Te}_{1-x}\text{W}_x)\text{O}_6$ retains the isostructural crystal lattice (tetragonal $I4/m$) over the full range of x . This rather rare property enables a wide tunability of J_2/J_1 . The parent compound $\text{Sr}_2\text{CuTeO}_6$, which shows Néel order at $T_N = 29$ K [19,20], has the exchange parameter $|J_2/J_1| = 0.03$ ($J_1 \simeq 88$ K) from the

*kchoi@cau.ac.kr

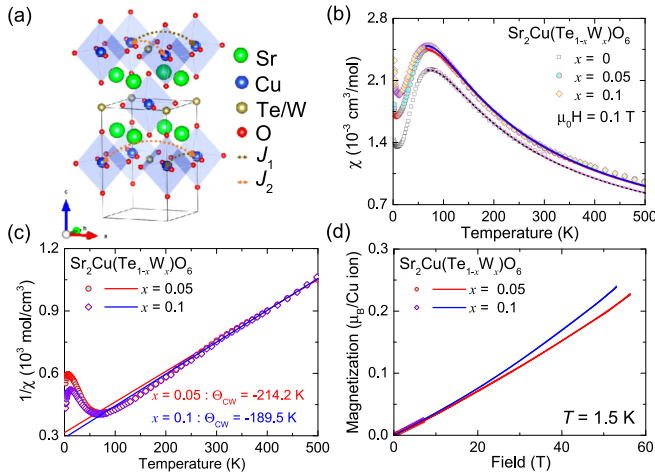


FIG. 1. (a) Crystal structure of $\text{Sr}_2\text{Cu}(\text{Te}_{1-x}\text{W}_x)\text{O}_6$ together with magnetic exchange interactions, J_1 and J_2 , on a square lattice (dot lines). The green, blue, dark yellow, and red spheres denote Sr, Cu, Te/W, and O ions, respectively. (b) dc magnetic susceptibility data $\chi(T)$ of $x = 0, 0.05$, and 0.1 as a function of temperature measured at $\mu_0 H = 0.1$ T. The solid lines represent the high-temperature extension fittings. (c) Inverse magnetic susceptibility of $x = 0.05$ and 0.1 as a function of temperature. The solid lines are fittings to the Curie-Weiss law. (d) High-field magnetization data of $x = 0.05$ and 0.1 measured at $T = 1.5$ K together with the low-field SQUID data (symbols).

renormalized parameters of inelastic neutron scattering data [21,22]. On the contrary, the other end member Sr_2CuWO_6 has the markedly different exchange parameter $|J_2/J_1| = 7.92$ ($J_1 \simeq 14$ K), leading to the columnar antiferromagnetic order at $T_N = 24$ K [23,24]. The drastically varying magnetic parameters and ground states between $x = 0$ and 1 are ascribed to the distinct orbital hybridization of the $\text{Te}^{6+}(4d^{10})$ and $\text{W}^{6+}(5d^0)$ ions with the $\text{O}^{2-}(2p^6)$ ion responsible for mediating the super-superexchange Cu-O-Te/W-O-Cu paths [22].

In previous works [18], a global phase diagram of $\text{Sr}_2\text{Cu}(\text{Te}_{1-x}\text{W}_x)\text{O}_6$ was determined. Remarkably, a quantum disordered state was observed in a wide composition range of $x = 0.1-0.7$ and was controversially discussed in terms of QSL versus valence-bond glass [16–18]. To date, thorough characterizations have been made only for the $x = 0.5$ sample that shows many aspects of the QSL phenomenology: a persistent spin dynamics down to 19 mK by muon spin relaxation and a T -linear dependence of low- T magnetic specific heat [16]. Nonetheless, the observed QSL-like phase over a wide range of x is not compatible with the theoretical prediction that supports QSL only in a narrow composition range of $x \simeq 0.23-0.33$ (corresponding to $|J_2/J_1| \simeq 0.4-0.6$). Rather, it is suggested that quenched disorders and local strains play a pivotal role in suppressing the magnetic ordering [7]. As such, the W^{6+} -for- Te^{6+} substitution seems to bring about a significant deformation of local superexchange paths in conjunction with exchange randomness due to their random occupation.

In addition to understanding the precise nature of the observed quantum disordered state at $x = 0.1-0.7$, less clear is spin dynamics in the vicinity of the phase boundary that separates the Néel ordered from the quantum disordered phase.

In this regard, we focus on the $x = 0.05$ and 0.1 compositions that lie close to the Néel critical end point to elucidate the impact of quenched disorders and frustration on an emergent QSL-like state.

In this paper, we employ multiple thermodynamic and magnetic resonance techniques to detect low-lying excitations of $\text{Sr}_2\text{Cu}(\text{Te}_{1-x}\text{W}_x)\text{O}_6$ ($x = 0.05$). It turns out that the 5% W^{6+} substitution for Te^{6+} is sufficient to suppress the Néel ordered state. We further identify an energy hierarchy of low-energy excitations through distinct power-law-like dependences of the specific heat and muon spin relaxation rates. In addition, our muon spin rotation data reveal a fraction of frozen magnetic moments in a random-singlet-like background. Our results suggest that a random-singlet-like state forms a low-energy landscape near the Néel phase boundary.

II. EXPERIMENTAL DETAILS

Polycrystalline samples of $\text{Sr}_2\text{Cu}(\text{Te}_{1-x}\text{W}_x)\text{O}_6$ ($x = 0, 0.05$, and 0.1) were synthesized by the solid-state reaction method as described in Refs. [16–18]. The mixture of SrCO_3 , CuO , TeO_2 , and WO_3 in the $2 : 1 : 1 - x : x$ molar ratio was ground in an agate mortar, and it was then calcined at 900°C . After the calcination, the powder was reground, pelletized, and sintered once at 1100°C . The phase purity of $\text{Sr}_2\text{Cu}(\text{Te}_{1-x}\text{W}_x)\text{O}_6$ was examined by the x-ray diffraction (XRD) method with Cu $K\alpha$ radiation. The XRD patterns of our samples agree with the previously reported results (not shown here) [18].

dc magnetic susceptibility and isothermal-magnetization measurements were performed using a VSM-SQUID (superconducting quantum interference device) magnetometer (MPMS3, Quantum Design). The magnetic susceptibilities were taken in the temperature range of $T = 2-300$ (500) K at $\mu_0 H = 0.1$ T for $x = 0$ ($x = 0.05$ and 0.1). Isothermal magnetization curves were measured up to 7 T at $T = 2$ K and were used for calibration of the high-field magnetization data. High-field magnetization measurements were carried out at the Dresden High Magnetic Field Laboratory with a nondestructive pulsed magnet. The magnetic moment was detected with a pickup coil device by sweeping the pulsed magnetic field up to 55 T at $T = 1.5$ K. The specific heat of the $x = 0.05$ compound was recorded using Physical Property Measurement System (PPMS, Quantum Design) with the thermal-relaxation method. Electron spin resonance (ESR) was measured by a conventional X-band ESR system (JEOL JES-RE3X). The ESR signals were recorded for $x = 0.05$ at $T = 4-200$ K using a continuous flow cryostat (ESR 900, Oxford Instruments).

Muon spin rotation and relaxation (μSR) measurements of $x = 0.05$ and 0.1 compounds were carried out on the ARGUS and CHRONUS spectrometers at the RIKEN-RAL Muon facility. Time-differential muon spin polarization sensitive to local magnetic fields was measured from $T = 0.3$ to 30 K and $T = 0.07$ to 40 K for $x = 0.05$ and 0.1 , respectively, at zero field and at several longitudinal fields up to 0.4 T. We further conducted muon spin rotation experiments of $x = 0.05$ in the temperature range of $T = 0.3-20$ K at a weak transverse field of 0.002 T. All of the obtained data were analyzed by the free software package WIMDA [25].

III. RESULTS AND DISCUSSION

A. Static magnetic susceptibility and high-field magnetization

Figure 1(b) exhibits dc magnetic susceptibilities $\chi(T)$ of $\text{Sr}_2\text{Cu}(\text{Te}_{1-x}\text{W}_x)\text{O}_6$ ($x = 0, 0.05, \text{ and } 0.1$) as a function of temperature. Our $\chi(T)$ data are consistent with the previously published data [16–18]. We observed no distinguishable kink or anomaly even for the pristine $\text{Sr}_2\text{CuTeO}_6$, which is known to order antiferromagnetically at $T_N = 29$ K [19–21]. Rather, $\chi(T)$ displays a broad maximum around $T_{\text{max}} = 70$ K for all the investigated compounds. This feature is associated with short-range magnetic order, characteristic for a two-dimensional square lattice [26–28]. As the W^{6+} concentration is increased, T_{max} slightly decreases from 75 K at $x = 0$ to 68 K at $x = 0.1$, while the height of $\chi(T_{\text{max}})$ is systematically enhanced. This trend is in accordance with the theoretically calculated $\chi(T)$ based on the J_1 - J_2 model [29–31].

We made a further analysis of $\chi(T)$ in terms of the high-temperature expansion formula [see the solid lines in Fig. 1(b) for the fitting curves] [32]. The obtained exchange interactions are $J_1 = 83.00$ K and $J_2 = 0.52$ K for $x = 0$, $J_1 = 82.57$ K and $J_2 = 3.24$ K for $x = 0.05$, and $J_1 = 81.38$ K and $J_2 = 8.36$ K for $x = 0.1$. It was found that magnetic exchanges of the $x = 0$ compound (black solid line) are similar to the previous data (short-dot line), $J_1 = 83.29$ K (7.18 meV) and $J_2 = 0.29$ K (0.025 meV) [21], as displayed in Fig. 1(b). Small differences of magnetic exchanges are thought to be due to the different calculation orders and temperature ranges. As expected, the W^{6+} substitution leads to the increase of J_2 .

We attempted fittings of $1/\chi(T)$ to the Curie-Weiss law in the high-temperature range of $T = 300$ – 500 K, as exhibited in Fig. 1(c). The extracted Weiss temperatures are $\Theta_{\text{CW}} = -214.2$ and -189.5 K for the $x = 0.05$ and 0.1 compounds, respectively. The large negative Θ_{CW} means dominant antiferromagnetic interactions of the Cu^{2+} spins. We note that our values of Θ_{CW} are roughly three times larger than the reported $\Theta_{\text{CW}} \approx -80$ to 60 K for the $x = 0$ and 0.1 – 0.7 compounds [18]. This discrepancy is caused by the fact that the previous analysis was made in a limited temperature interval between $T = 250$ and 300 K, which is not wide enough to obtain the reliable Curie-Weiss parameters.

With increasing x , a Curie-like upturn and a low- T residual contribution become pronounced. The Curie-like tail is associated with weakly interacting orphan spins. The Curie fit to the low- T $\chi(x)$ places an upper limit on the concentration of the orphanlike spins of about 0.3%. The broad feature suggests that the W^{6+} substitution creates abundant low-energy states. We recall that the chemical substitution in $\text{Sr}_2\text{Cu}(\text{Te}_{1-x}\text{W}_x)\text{O}_6$ induces a drastic change of the exchange interaction parameters because the delocalized $\text{W}^{6+}(5d^0)$ orbital strongly hybridizes with $\text{O}^{2-}(2p^6)$ [22]. This renders the 180° Cu-O-W-O-Cu superexchange path active, which is nearly disconnected for $x = 0$. As a result, the introduction of the W^{6+} ion enhances exchange frustration by increasing the J_2 diagonal interaction, while concomitantly creating exchange randomness and local strains.

Figure 1(d) shows the high-field magnetization $M(H)$ curves of $x = 0.05$ and 0.1 measured at $T = 1.5$ K with a pulsed field magnet up to 55 T. $M(H)$ at 50 T amounts to approximately $0.2\mu_B/\text{Cu}^{2+}$ ion. With increasing W^{6+}

concentration, $M(H)$ is systematically enhanced in the whole measured field range, being consistent with the $\chi(T)$ data [see Fig. 1(b)]. Noticeably, $M(H)$ shows a concave curvature. In classical antiferromagnets, we expect a linear field dependence. As the Cu^{2+} ions have negligible anisotropies, the concave curvature is ascribed to quantum fluctuations. For a two-dimensional spin system, the nonlinear correction to the linear term results from a gradual suppression of zero-point fluctuations by an external field [33]. We tried to describe the magnetization using the expression $M(H) \sim \chi_M H + (2/\pi)(H/H_c)^2$, where H_c is the saturation field. The extracted fit parameters are $\chi_M \sim 3.27 \times 10^{-3}$ (cm^3/mol) and $H_c \sim 219$ T for $x = 0.05$ and $\chi_M \sim 3.37 \times 10^{-3}$ (cm^3/mol) and $H_c \sim 173$ T for $x = 0.1$. Noticeably, the calculated saturation fields H_c agree well with the Curie-Weiss temperatures Θ_{CW} , confirming the validity of our analysis and that the quantum fluctuations are responsible for the nonlinear $M(H)$. The obtained χ_M increases systematically with x while the saturation field decreases. However, the magnitude of χ_M ($T = 1.5$ K) is larger than the dc χ_{dc} ($T = 2$ K) values of $\chi \sim 1.81$ and 2.31×10^{-3} (cm^3/mol) for $x = 0.05$ and 0.1 , respectively. The discrepancy is partly due to the lower measured temperature of $M(H)$ than $\chi_{\text{dc}}(T)$.

B. Specific heat of the $x = 0.05$ compound

To elucidate the nature of low-energy excitations, specific-heat measurements of the $x = 0.05$ compound were carried out at $T = 0.3$ – 160 K. Figure 2(a) presents a log-log plot of the specific heat versus temperature at selected fields $\mu_0 H = 0, 5, \text{ and } 9$ T. We observe no λ -like anomaly. In addition, we stress that neither a Schottky hump nor a low- T maximum is observed, suggesting that neither the orphan spins nor valence-bond solids contribute to the low- T specific heat. As the temperature is lowered toward 0 K, the specific heat monotonically decreases with its slope changes. With increasing magnetic field to 9 T, there appears a discernible redistribution of the specific heat through 2 K. The reduction of the specific heat below 2 K is compensated by the increase of the specific heat between 2 and 15 K. Overall, the specific heats of the $x = 0.05$ and 0.1 compounds look alike, which is more enhanced than that of the pristine sample [16–18]. This suggests that the small W^{6+} substitution generates abundant low-energy excitations and that the $x = 0.05$ and 0.1 compounds share a similar ground state.

We single out the magnetic contribution of the specific heat divided by temperature C_{mag}/T by subtracting the lattice contribution [solid line in Fig. 2(b)] from the raw data. To estimate the lattice contribution, a nonmagnetic counterpart $\text{Sr}_2\text{Zn}(\text{Te}_{1-x}\text{W}_x)\text{O}_6$ ($x = 0.05$) is used with the Bouvier method [34]. In Fig. 2(c), we present a log-log plot of C_{mag}/T versus temperature.

For temperatures below $T_1 = 15$ K, the C_{mag}/T data are described by a power-law-like behavior T^α , where α is the exponent. On cooling through $T_2 = 4.5$ K, C_{mag}/T changes the exponent from $\alpha = 0.37$ to 0.09 and from $\alpha = 0.09$ to 1.2 through $T_3 = 0.9$ K. Namely, C_{mag} follows the $T^{1.4}$ -dependence between T_1 and T_2 , the $T^{1.1}$ -dependence between T_2 and T_3 , and the $T^{2.2}$ -dependence below T_3 . Here, we stress that the T -linear dependence in the limited T range

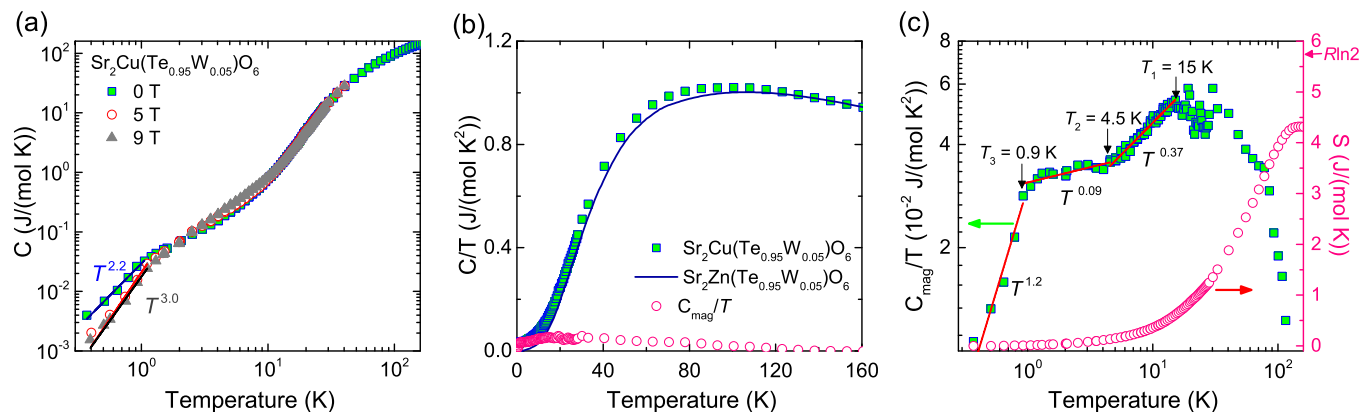


FIG. 2. (a) Low-temperature dependence of the specific heat of $\text{Sr}_2\text{Cu}(\text{Te}_{1-x}\text{W}_x)\text{O}_6$ ($x = 0.05$) at selected fields $\mu_0 H = 0, 5,$ and 9 T plotted in a double logarithmic scale. (b) Specific heat divided by temperature together with the nonmagnetic counterpart $\text{Sr}_2\text{Zn}(\text{Te}_{0.95}\text{W}_{0.05})\text{O}_6$. The magnetic specific heat divided by temperature C_{mag}/T (red open circles) is obtained by subtracting the nonmagnetic contribution from the raw C/T data. (c) Log-log plot of C_{mag}/T vs temperature. The solid lines are fits of the C_m/T data to a power law, and the red open symbols represent the magnetic entropy.

should be considered a guide to the eye, although the T -linear dependence is observed in the specific heat of $x = 0.1$ – 0.5 in a similar temperature range [16–18]. On the other hand, the parent compound $\text{Sr}_2\text{CuTeO}_6$ shows the quadratic T -dependence, pertaining to quasi-two-dimensional magnetic excitations [16–19]. Generically speaking, the quadratic behavior has often been reported in the $s = 1$ triangular lattices NiGa_2S_4 and $\text{Ba}_3\text{NiSb}_2\text{O}_9$ as well as the $j_{\text{eff}} = 1/2$ hyperkagome iridate $\text{Na}_4\text{Ir}_3\text{O}_8$ [35–37]. At any rate, the successive power-law-like dependence with $\alpha < 3$ implies an energy hierarchy of low-energy excitations and a substantial gapless magnetic contribution to the specific heat. The magnetic entropy is calculated from the integration of C_{mag} . The magnetic entropy reaches 4.32 J/(mol K) at 160 K, which amounts to about $3/4$ of $R \ln(2s + 1)$ for $s = 1/2$. The lacking magnetic entropy may be due to a slight overestimation of the lattice contribution.

C. Electron spin resonance of the $x = 0.05$ compound

We performed electron spin resonance (ESR) measurements of the $x = 0.05$ compound to extract information about the evolution of spin correlations. Figure 3(a) exhibits the selected ESR spectra in the temperature interval between 4 and 200 K measured at $\nu = 9.12$ GHz. In the high- T paramagnetic state, the ESR spectrum is well described by a convolution of two Lorentzian profiles, typical for the Cu^{2+} ions in the tetragonal structure. The Lorentzian line shape suggests that the ESR signal is exchange-narrowed due to the fast electronic fluctuations of the Cu^{2+} spins coupled by the strong exchange interactions of $J_1 \simeq 88$ K and $J_2 \simeq 7.0$ K for the $x = 0$ [20,21].

With decreasing temperature, the ESR signal progressively broadens. To quantify the ESR parameters as a function of temperature, the powder ESR spectra were fitted to a sum of the derivative of two Lorentzian profiles [see the thin lines in Fig. 3(a)]. By tracking the two components of the ESR signals, we find that the ESR spectra undergo a qualitative change on cooling through $T_1 = 15$ K. We recall that $C_{\text{mag}}(T)$ starts to exhibit the power-law-like dependence at this temperature.

More specifically, the two equally intense signals are observed down to T_1 . The two absorption lines emerge into a single one below T_1 , while an additional sharp peak (denoted by the asterisk) shows up. The latter new peak may be associated with the weakly coupled orphanlike spins, judging from the fact that the effective g -factor is close to $g \approx 2$, and its intensity first decreases and then changes to a steep increase with decreasing temperature (not shown here). In a bond-disorder-induced random singlet, the orphanlike spins are an intrinsic entity coexisting with a broad distribution of valence bonds. On top of the random singlet, isolated spins can be

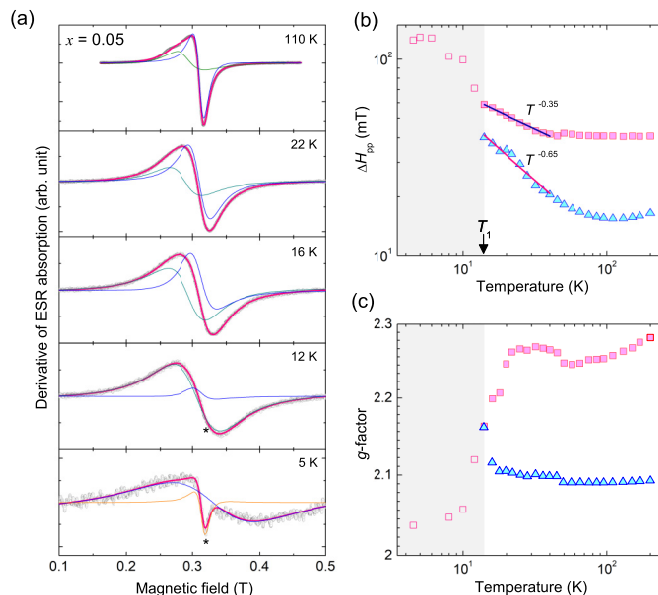


FIG. 3. (a) Derivative of the ESR absorption spectra for the $x = 0.05$ compound at selected temperatures. The ESR spectra are fitted to a sum (pink thick line) of two Lorentzian profiles (thin solid lines). (b) Log-log plot of the peak-to-peak linewidth ΔH_{pp} vs temperature. The solid lines represent a power-law fit. (c) Log-log plot of the g -factors as a function of temperature. The gray shading marks a qualitative change of the ESR spectra.

generated by defects, and magnetic clusters can also emerge in the phase boundary of the Néel-to-disordered transition. As such, the sharp low- T peak may contain both extrinsic and intrinsic signals to the random singlet. We further note that at $T = 5$ K, the intensity of the sharp signal amounts to less than 10% of the broad peak. Thus, the random singlet dominates a low-energy physics of the $x = 0.05$ and 0.1 compounds.

Figures 3(b) and 3(c) show the temperature dependencies of the peak-to-peak linewidth, ΔH_{pp} , and the g -factor, respectively. $\Delta H_{pp}(T)$ is largely independent of temperature above 50–80 K. In the intermediate temperature between T_1 and $T = 50$ –80 K, $\Delta H_{pp}(T)$ follows a critical power law $T^{-0.35}$ for the $H \parallel ab$ -plane and $T^{-0.65}$ for $H \parallel c$. The critical-like line broadening is due to the development of short-range spin correlations, associated with the broad maximum in $\chi(T)$ [see Fig. 1(b)]. The notable thing is that the ΔH_{pp} anisotropies become smaller as $T \rightarrow T_1$. Eventually, the two separated signals coalesce into the single signal at T_1 , indicative of the disappearance of the apparent anisotropy. The merged signal shows a strong broadening below T_1 and then becomes temperature-independent below 6 K. At $T = 200$ K we determine the g -factors $g_{ab} = 2.3$ and $g_c = 2.1$. These values are typical for the Cu^{2+} ion in the tetragonal structure: $g_{ab} = 2 - \frac{8\lambda_{SO}}{\Delta}$ and $g_c = 2 - \frac{2\lambda_{SO}}{\Delta}$ (λ denotes spin-orbit coupling and Δ is the crystal-field splitting). With decreasing temperature, g_c gradually increases toward 2.17. In contrast, g_{ab} shows a nonmonotonic behavior. On cooling, g_{ab} slightly decreases and then forms a broad hump and finally drops to 2.17 at T_1 . The broad hump of the in-plane effective g -factor is linked to the buildup of short-range local fields. Then, the drop means the cancellation of the local staggered field. It is remarkable that the anisotropy of the effective g -factors disappears below T_1 and that the effective g -factor is substantially renormalized to 2.05. This implies that the spins in the low- T magnetic state ($T \leq T_1$) are no longer critically fluctuating, yet they behave like quantum paramagnets.

Given the intriguing evolution of $\Delta H_{pp}(T)$ and the g -factor, the short-range correlated state evolves into an exotic quantum state below T_1 . Since there is no structural phase transition, the anomalous behaviors of $\Delta H_{pp}(T)$ and the g -factor are of magnetic origin. As the low- T ESR spectra comprise the sharp and broad components whose effective g -factors are close to 2 of a free spin, the ground state may consist of the nearly free spins, random-singlet-like spins, and magnetic clusters.

D. Muon spin rotation and relaxation

As the magnetic susceptibility and specific heat are largely insensitive to long-range magnetic order, we employed μSR techniques to examine the absence of long-range order in the vicinity of the Néel critical end point. Since surface muons are 100% polarized with a large gyromagnetic ratio of $\gamma_\mu = 2\pi \times 135.5$ MHz/T, μSR serves as an extremely sensitive probe of sensing tiny local magnetic fields of $\sim 10^{-4}$ T in their static and dynamic forms. We carried out μSR measurements of $\text{Sr}_2\text{Cu}(\text{Te}_{1-x}\text{W}_x)\text{O}_6$ ($x = 0.05$ and 0.1) at zero field, at a weak transverse field of 0.002 T, and at several longitudinal fields. The temperature was varied between 0.3 and 0.07 K up to 40 K for the $x = 0.05$ and 0.1 compounds, respectively. The time evolution of muon spin polarization, $P(t)$, obtained

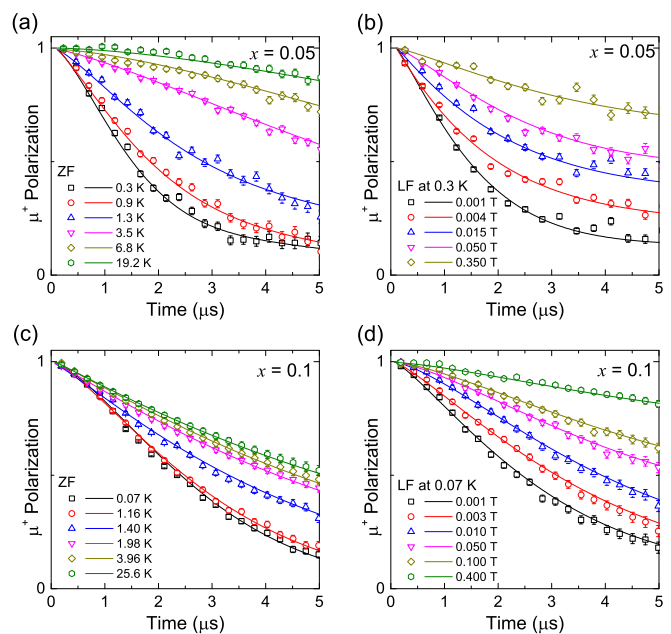


FIG. 4. Temperature evolution of the muon spin polarization for $\text{Sr}_2\text{Cu}(\text{Te}_{1-x}\text{W}_x)\text{O}_6$ ($x = 0.05$) at zero field (a) and at longitudinal fields (b), and for the $x = 0.1$ compound at zero field (c) and at longitudinal fields (d). The solid lines are fits to Eq. (1) as explained in the main text.

at zero field and at several longitudinal fields is summarized in Fig. 4 at several temperatures.

As shown in Figs. 4(a) and 4(c), the oscillations of $P(t)$ are apparently lacking, which arise from the static magnetic field experienced by the muon spin. This confirms that both compounds do not show any long-range order. We note that the μSR data of $x \approx 0.1$ –0.6 were limited above 1 K in the previous study [18]. For temperatures above 1.5 K, our zero-field data of the $x = 0.1$ compound are consistent with the earlier result [18]. As our μSR data extend the measured temperature down to 0.07 K and include longitudinal-field (LF) measurements, we are able to refine a ground state. A close look at the $x = 0.05$ μSR spectra reveals a slight loss of the initial $P(t)$ at low temperatures (see Fig. 6). This feature might indicate the presence of frozen magnetic moments, which are obviously absent for $x = 0.1$. Since we observe no 1/3-tail of $P(t)$ at long times, it is improbable that the frozen magnetic moments occupy an entire sample to form spin-glass-like freezing. Rather, both compounds are still dominated by dynamic magnetism.

Additional evidence for the dynamic character of electronic magnetic moments is provided by μSR measurements in a longitudinal magnetic field. When the longitudinal field is applied parallel to the initial muon spin direction, $P(t)$ induced by local static fields is decoupled. If the LF is stronger than roughly 10 times the internal field, the time-differential $P(t)$ fully saturates [38]. As shown in Figs. 4(b) and 4(d), however, the muon spin polarization is strongly dependent on time in the LF up to 0.4 T, suggesting that the transverse components of local magnetic fields are fluctuating at all temperatures down to $T = 0.3$ and 0.07 K for $x = 0.05$ and 0.1, respectively.

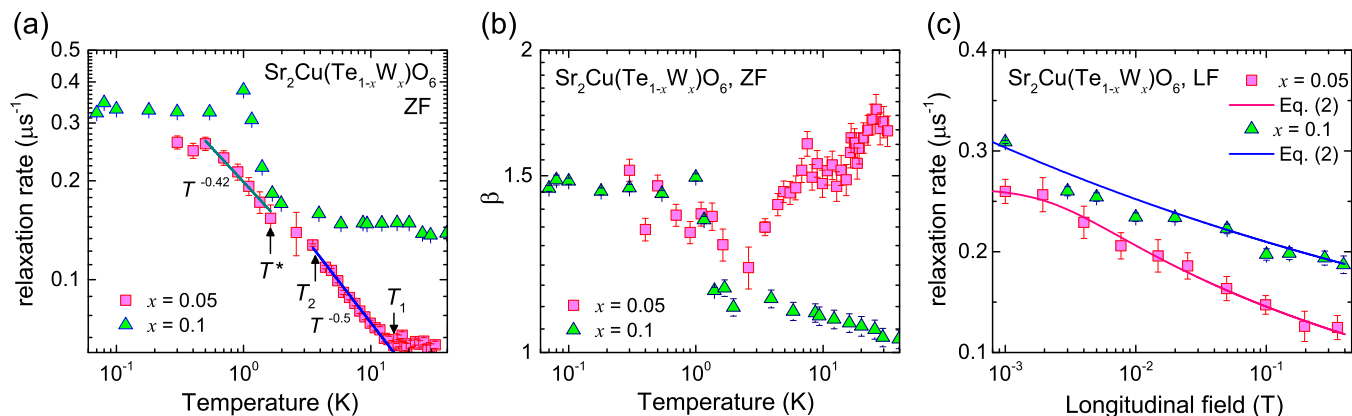


FIG. 5. (a) Log-log plots of the muon spin relaxation rate vs temperature for $\text{Sr}_2\text{Cu}(\text{Te}_{1-x}\text{W}_x)\text{O}_6$ ($x = 0.05$ and 0.1) measured at zero field. Linear solid lines are fits to the power law. (b) Stretching exponent of $x = 0.05$ and 0.1 plotted in a double logarithmic scale. (c) Longitudinal-field dependence of the muon spin relaxation rate at $T = 0.3$ and 0.07 K for $x = 0.05$ and 0.1 compounds, respectively, together with their fits to Eq. (2).

To extract the relaxation rate from the time-differential $P(t)$, we fit the ZF- and LF- μSR data to a stretched exponential relaxation function

$$P(t) = P_{\text{bg}} + P_1 \exp[-(\lambda t)^\beta], \quad (1)$$

where P_1 is the relaxing amplitude, λ is the muon relaxation rate induced by the Cu^{2+} magnetic moments, and β is the stretching exponent. The P_{bg} term stands for a background contribution, originating from the sample holder or the cryostat surrounding the sample space. It is independent of temperature with values of approximately 0.1 and 0.15 for $x = 0.05$ and 0.1 , respectively. The stretched exponential function is usually used as a phenomenological description of the distribution of relaxation times in a disordered system. Further, we recall that this fitting function is applied to describe the spin dynamics of low-dimensional systems, including a kagome-lattice antiferromagnet $\text{SrCr}_8\text{Ga}_4\text{O}_{19}$, a Haldane material $(\text{Y}_{2-x}\text{Ca}_x)\text{Ba}(\text{Ni}_{1-y}\text{Mg}_y)\text{O}_5$, a triangle-based iridate $\text{Ba}_3\text{IrTi}_2\text{O}_9$ [39–41], and $\text{Sr}_2\text{Cu}(\text{Te}_{1-x}\text{W}_x)\text{O}_6$ ($x = 0.1$ – 0.6) [16,18]. The resulting $\lambda(T)$ as a function of temperature and longitudinal field are displayed in Figs. 5(a) and 5(c), respectively.

As plotted in Fig. 5(a), $\lambda(T)$ of $x = 0.05$ starts to increase on cooling down below T_1 and then becomes constant for

temperatures below 0.5 K. In a wide crossover temperature between 0.5 and 15 K, $\lambda(T)$ is described by a power-law-like dependence with a weak slope change between $T^* = 1.6$ K and T_2 . As to the $x = 0.1$ compound, the crossover regime shrinks, and its onset temperature shifts to 2 K, while the plateau appears at 1 K. We comment that both compounds reveal the persistent spin dynamics below $T = 0.5$ – 1 K, which is often observed in the frustrated magnets showing spin freezing, weak magnetic order, or quantum spin liquid [42–48]. Furthermore, it should be mentioned that the high- T $\lambda(T)$ of $x = 0.1$ is more than three times larger than that of $x = 0.05$, and that $\lambda(T)$ increases with increasing x in the persistent spin dynamics region [16]. It means that the persistent spin dynamics is proportionally augmented to the W^{6+} concentration.

In the fast-fluctuation paramagnetic limit, the relaxation rate is given by $\lambda = 2\Delta^2/\nu$ with the Cu^{2+} spin fluctuation rate ν and the field distribution width Δ . Using the nearest-neighbor coordination number $z = 4$ of the $s = 1/2$ square lattice and $J_1 \simeq 88$ K, we calculate the exchange fluctuation rate $\nu = \sqrt{z}J_1S/\hbar \approx 1.2 \times 10^{13}$ Hz [39,46,49]. Given that the exchange interactions hardly change by the small W^{6+} substitution, the enhanced high- T $\lambda(T)$ of $x = 0.1$, compared to $x = 0.05$, is interpreted as a significant broadening of the internal field distribution. From the value of $\lambda(T)$ at the lowest

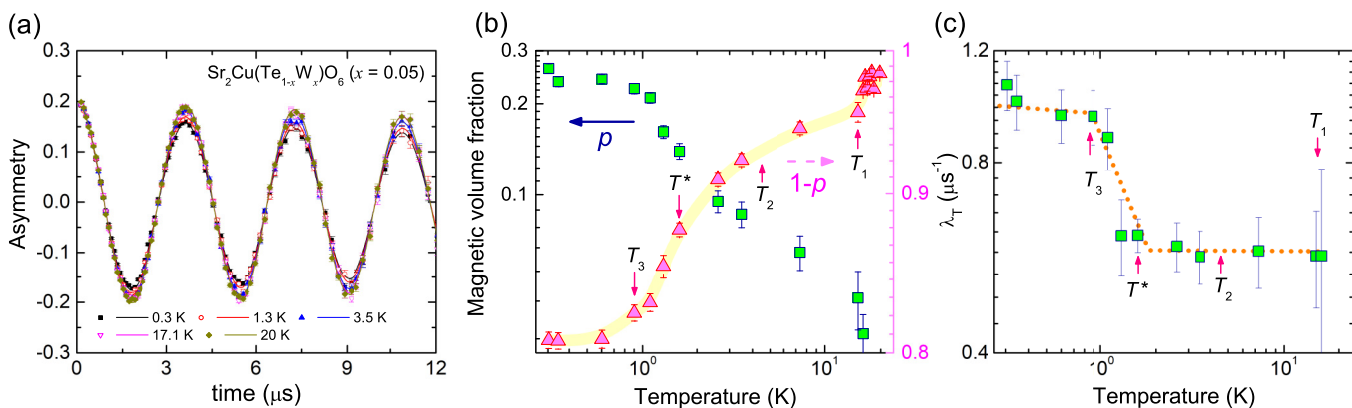


FIG. 6. (a) Temperature evolution of the μSR spectra for the compound $\text{Sr}_2\text{Cu}(\text{Te}_{1-x}\text{W}_x)\text{O}_6$ ($x = 0.05$) at a weak transverse field of 0.002 T. (b) Magnetic volume fraction and (c) transverse muon spin relaxation rate as a function of temperature plotted on a log-log scale.

measured temperature, we estimate the local magnetic field as 3.17×10^{-4} T for $x = 0.05$ and 3.64×10^{-4} T for $x = 0.1$. If the estimated local fields were solely due to static fields, the full polarization of the LF- μ SR spectra is expected at a longitudinal field of ~ 40 G through a spin-locking effect [38]. However, the absence of the complete decoupling lends further support for a dynamic ground state in the muon time window.

In addition, the T -dependence of the stretching exponent, $\beta(T)$, reveals a distinct behavior between $x = 0.05$ and 0.1. Overall, $\beta(T)$ of $x = 0.1$ resembles $\lambda(T)$ while increasing from 1 to 1.6 with decreasing temperature. A similar trend has been reported in the $x = 0.5$ compound and $\text{SrCr}_8\text{Ga}_4\text{O}_{19}$ [16,39]. In sharp contrast, $\beta(T)$ of $x = 0.05$ decreases from 1.8 to 1.3 as the temperature is lowered down to $T \sim 25$ K. The origin of the contrasting high- T $\beta(T)$ between $x = 0.05$ and 0.1 is far from clear. Below 20 K, $\beta(T)$ of both $x = 0.05$ and 0.1 parallel each other. Noticeably, the low- T $\beta(T)$ of both compounds is between that of a Gaussian and Lorentzian relaxation function. Generally speaking, a Gaussian-like distribution is expected for dense disordered systems, while a Lorentzian-like distribution is expected for dilute systems [38]. In a specific case, the Gaussian form of the relaxation function can arise from migrating unpaired spins in the matrix of singlet spins [39]. In consideration of this, the ground state of $x = 0.05$ and 0.1 is largely compatible with the random singlet picture comprising resonating singlets and propagating orphanlike spins.

Shown in Fig. 5(c) is $\lambda_{\text{LF}}(H)$ measured at $T = 0.3$ and 0.07 K for $x = 0.05$ and 0.1, respectively. With increasing LF, $\lambda_{\text{LF}}(H)$ first decreases rapidly and then almost levels out above 0.1 T. We try to describe $\lambda_{\text{LF}}(H)$ based on a general spin autocorrelation function, $S(t) \sim t^{-r} \exp(-\nu t)$, where r is the critical exponent [46,49–51]. In this case, the muon spin relaxation rate can be expressed as

$$\lambda(H) \sim \int_0^{\infty} t^{-r} \exp(-\nu t) \cos(\gamma_{\mu} H t) dt. \quad (2)$$

A reasonable description of the relaxation data is obtained using the parameters $r = 0.85$ (0.92) and $\nu = 2.0 \times 10^6$ Hz (1.0×10^5 Hz) for $x = 0.05$ (0.1). Compared to the high- T paramagnetic value of $\nu \approx 1.2 \times 10^{13}$ Hz, the reduction of the low- T ν demonstrates a substantial slowing down of the Cu^{2+} spin fluctuations. In addition, ν decreases by one order of magnitude with increasing x from 0.05 to 0.1. This suggests that an increasing W^{6+} concentration tends to promote dynamic spin fluctuations.

Lastly, we performed the muon spin rotation experiment in a weak transverse field (wTF) of 0.002 T to clarify possible inhomogeneous magnetism of $x = 0.05$. The wTF- μ SR spectra at selected temperatures are exhibited in Fig. 6(a). We find that the muon spin asymmetry measured at $T = 0.3$ K displays two distinct oscillation components, but the $T = 20$ K data reveal a single oscillation. With decreasing temperature, the damping rate gradually increases. The wTF- μ SR data are described by the model consisting of a sum of two cosine functions subject to an exponential damping,

$$A(t) = A_0 [p e^{-\lambda_T t} \cos(\omega_1 t + \phi_1) + (1-p) \times e^{-\lambda_{\text{bg}} t} \cos(\omega_2 t + \phi_2)], \quad (3)$$

where A_0 is the initial muon spin asymmetry, and p and $(1-p)$ are the magnetic volume fractions of frozen and paramagnetic-like states, respectively. λ_T is the transverse muon spin relaxation rate, $\omega_{1,2} = \gamma_{\mu} B_{1,2}$ are the Larmor angular frequencies, and $\phi_{1,2}$ are the initial phases, which are in the range of 0° – 10° . Here, the second cosine component describes a purely paramagnetic contribution as well as the background. In doing this, we neglect a small depolarizing contribution in the background with the order of $\lambda_{\text{bg}} \sim 10^{-3} \mu\text{s}^{-1}$, because it is too weak to affect the time range to be considered.

The T -dependence of the magnetic volume fractions, p and $(1-p)$, is shown in Fig. 6(b). As the temperature is lowered from T_1 , $(1-p)$ decreases stepwise, while showing the characteristic changes at T_1 , $T^* = 1.6$ K, and T_3 . Below T_3 , $(1-p)$ becomes saturated to the level of 80% of the whole volume fraction. This means that a minority of the Cu^{2+} spins is in the magnetically frozen state. As evident from the comparison between λ in Fig. 5(a) and λ_T in Fig. 6(c), λ_T is more than three times larger than λ . Consistently, a recent neutron diffraction study shows the presence of short-range Néel order [52]. The λ relaxation is of purely dynamical origin because λ_T is dominated by the development of the frozen magnetic fraction, as can be justified by the resemblance between p in Fig. 6(b) and λ_T in Fig. 6(c). λ_T is nearly temperature-independent down to $T^* = 1.6$ K, then it increases steeply toward T_3 , and finally it saturates below T_3 . Both p and λ_T hardly change through T_2 .

E. Discussion

We now discuss the implication of our results on a ground state. A comprehensive study of $\text{Sr}_2\text{Cu}(\text{Te}_{1-x}\text{W}_x)\text{O}_6$ ($x = 0.05$ and 0.1) sheds light on a spatiotemporal structure of low-lying excitations near the Néel phase boundary.

Surprisingly, the Néel AF order is drastically suppressed even in $x = 0.05$. Essentially the same conclusion is drawn by Hong *et al.* [52]. This extends the phase boundary of the quantum disordered state previously known as $x = 0.1$ – 0.7 down to $x = 0.05$. As mentioned above, the extreme efficiency of the W^{6+} substitution in suppressing the Néel order lies in the different hybridization mechanism of the Te^{6+} ($4d^{10}$) and W^{6+} ($5d^0$) orbitals with the O^{2-} ($2p^6$) orbital [22]. The key impact of the W^{6+} -for- Te^{6+} substitution is to switch on the diagonal interaction J_2 , thereby generating the competition between the J_1 -dominated Néel order and the J_2 -dominated columnar order. The randomness-induced low-energy density of states is nicely captured by the magnetic specific heat [see Fig. 2(c)], which is centered at a temperature of $J_2 \simeq 20$ K.

The low- T magnetic specific heat of $x = 0.05$ details the nature of emergent low-lying excitations. The power-law-like dependence $C_{\text{mag}} \sim T^\alpha$ ($1 \lesssim \alpha \lesssim 2$) appears with the characteristic temperatures $T_1 = 15$ K, $T_2 = 4.5$ K, and $T_3 = 0.9$ K. The onset temperature T_1 is comparable to the diagonal interaction $J_2 \simeq 20$ K. Further, we note that C_{mag} features the quadratic T -dependence observed in the parent compound $\text{Sr}_2\text{CuTeO}_6$ [16–19]. Below $T_1 = 15$ K, both ESR and μ SR provide a large degree of evidence that the $x = 0.05$ system enters a crossover regime, in which the magnetic state is understood as randomness-induced random singlets. The key ingredient of the random singlets is a mixture of nearly freely

propagating spins and spin singlets that have a broad distribution of their bond length and distance. The emergence of the two ESR signals at T_1 together with their g -factors close to the free-spin value is compatible with the random-singlet picture.

In addition, $w\text{TF-}\mu\text{SR}$ detects the development of magnetic volume fraction below T_1 , indicative of the presence of some inhomogeneity. This can be ascribed to the influence of random local strain induced by the substituted W^{6+} ions, thereby bringing about small lattice and magnetic deformations. Based on the almost T^2 -dependence of C_{mag} that is seen below T_3 in the pristine $\text{Sr}_2\text{CuTeO}_6$, we conclude that a minority of the short-range Néel ordered clusters are imbedded into the random-singlet background. Assuming the narrow ESR signal below T_1 is due to the orphan spins and the magnetic clusters, the intensity ratio of the sharp to the broad ESR signal places an upper limit on the 10% volume fraction for the magnetic clusters (and the orphan spins). Thus, the quantum disordered ground state of $x = 0.05$ is dominated by the random singlets.

IV. CONCLUSION

To conclude, combining bulk magnetization, specific heat, ESR, and μSR techniques, we have drawn the landscape of

low-energy excitations, focusing on the phase boundary of $\text{Sr}_2\text{Cu}(\text{Te}_{1-x}\text{W}_x)\text{O}_6$ ($x = 0.05$ and 0.1).

Our experimental results reveal that low-energy excitations of $x = 0.05$ contain the response mainly from random-singlet-like spins. This highlights a drastic impact of the W^{6+} -for- Te^{6+} substitution in generating random-bond J_1 - J_2 interactions. These findings give an elaborate perspective for a spin-liquid-like state emergent near the Néel ordered phase boundary in frustrated magnets subject to quenched disorders.

ACKNOWLEDGMENTS

The work at CAU was supported by the National Research Foundation (NRF) of Korea (Grants No. 2020R1A2C3012367 and No. 2013M7A1A1075764). We acknowledge the support of the HLD at HZDR, a member of the European Magnetic Field Laboratory (EMFL). We acknowledge support from the liquid helium facility at IISER Mohali. We also acknowledge RIKEN and the STFC for providing access to muon beam time. F.C.C. acknowledges funding support from the Ministry of Science and Technology in Taiwan (Grants No. 106-2119-M-002-035-MY3 and No. 108-2622-8-002-016), the Ministry of Education in Taiwan (Grant No. AI-MAT-108L900903), and Academia Sinica (Grant No. AS-iMATE-108-11). The ESR work in RIKEN was supported by JSPS KAKENHI Grant No. JP19K06606.

-
- [1] K. Watanabe, H. Kawamura, H. Nakano, and T. Sakai, *J. Phys. Soc. Jpn.* **83**, 034714 (2014).
 - [2] H. Kawamura, K. Watanabe, and T. Shimokawa, *J. Phys. Soc. Jpn.* **83**, 103704 (2014).
 - [3] T. Shimokawa, K. Watanabe, and H. Kawamura, *Phys. Rev. B* **92**, 134407 (2015).
 - [4] I. Kimchi, A. Nahum, and T. Senthil, *Phys. Rev. X* **8**, 031028 (2018).
 - [5] I. Kimchi, J. P. Sheckelton, T. M. McQueen, and P. A. Lee, *Nat. Commun.* **9**, 4367 (2018).
 - [6] L. Liu, H. Shao, Y.-C. Lin, W. Guo, and A. W. Sandvik, *Phys. Rev. X* **8**, 041040 (2018).
 - [7] K. Uematsu and H. Kawamura, *Phys. Rev. B* **98**, 134427 (2018).
 - [8] S. T. Rodan, S. Yoon, S. Lee, K.-Y. Choi, G. Kim, J.-S. Rhyee, A. Koda, W.-T. Chen, and F. Chou, *Phys. Rev. B* **98**, 214412 (2018).
 - [9] S.-H. Do, C. H. Lee, T. Kihara, Y. S. Choi, S. Yoon, K. Kim, H. Cheong, W.-T. Chen, F. Chou, H. Nojiri, and K.-Y. Choi, *Phys. Rev. Lett.* **124**, 047204 (2020).
 - [10] P. W. Anderson, *Science* **235**, 1196 (1987).
 - [11] E. Dagotto and A. Moreo, *Phys. Rev. Lett.* **63**, 2148 (1989).
 - [12] R. Darradi, O. Derzhko, R. Zinke, J. Schulenburg, S. E. Krüger, and J. Richter, *Phys. Rev. B* **78**, 214415 (2008).
 - [13] H.-C. Jiang, H. Yao, and L. Balents, *Phys. Rev. B* **86**, 024424 (2012).
 - [14] L. Wang and A. W. Sandvik, *Phys. Rev. Lett.* **121**, 107202 (2018).
 - [15] S. Vasala, J.-G. Cheng, H. Yamauchi, J. B. Goodenough, and M. Karppinen, *Chem. Mater.* **24**, 2764 (2012), and references therein.
 - [16] O. Mustonen, S. Vasala, E. Sadrollahi, K. P. Schmidt, C. Baines, H. C. Walker, I. Terasaki, F. J. Litterst, E. Baggio-Saitovitch, and M. Karppinen, *Nat. Commun.* **9**, 1085 (2018).
 - [17] M. Watanabe, N. Kurita, H. Tanaka, W. Ueno, K. Matsui, and T. Goto, *Phys. Rev. B* **98**, 054422 (2018).
 - [18] O. Mustonen, S. Vasala, K. P. Schmidt, E. Sadrollahi, H. C. Walker, I. Terasaki, F. J. Litterst, E. Baggio-Saitovitch, and M. Karppinen, *Phys. Rev. B* **98**, 064411 (2018).
 - [19] T. Koga, N. Kurita, and H. Tanaka, *J. Phys. Soc. Jpn.* **83**, 115001 (2014).
 - [20] T. Koga, N. Kurita, M. Avdeev, S. Danilkin, T. J. Sato, and H. Tanaka, *Phys. Rev. B* **93**, 054426 (2016).
 - [21] P. Babkevich, V. M. Katukuri, B. Fåk, S. Rols, T. Fennell, D. Pajić, H. Tanaka, T. Pardini, R. R. P. Singh, A. Mitrushchenkov, O. V. Yazyev, and H. M. Rønnow, *Phys. Rev. Lett.* **117**, 237203 (2016).
 - [22] V. M. Katukuri, P. Babkevich, O. Mustonen, H. C. Walker, B. Fåk, S. Vasala, M. Karppinen, H. M. Rønnow, and O. V. Yazyev, *Phys. Rev. Lett.* **124**, 077202 (2020).
 - [23] S. Vasala, M. Avdeev, S. Danilkin, O. Chmaissem, and M. Karppinen, *J. Phys. Condens. Matter* **26**, 496001 (2014).
 - [24] H. C. Walker, O. Mustonen, S. Vasala, D. J. Voneshen, M. D. Le, D. T. Adroja, and M. Karppinen, *Phys. Rev. B* **94**, 064411 (2016).
 - [25] F. L. Pratt, *Physica B* **289-290**, 710 (2000).
 - [26] L. J. de Jongh and A. R. Miedema, *Adv. Phys.* **23**, 1 (1974).
 - [27] J. K. Kim and M. Troyer, *Phys. Rev. Lett.* **80**, 2705 (1998).
 - [28] H. Rosner, R. R. P. Singh, W. H. Zheng, J. Oitmaa, and W. E. Pickett, *Phys. Rev. B* **67**, 014416 (2003).
 - [29] N. Shannon, B. Schmidt, K. Penc, and P. Thalmeier, *Eur. Phys. J. B* **38**, 599 (2004).

- [30] J. Richter, A. Lohmann, H.-J. Schmidt, and D. C. Johnston, *J. Phys. Conf. Ser.* **529**, 012023 (2014).
- [31] J. Richter, P. Müller, A. Lohmann, and H.-J. Schmidt, *Phys. Proc.* **75**, 813 (2015).
- [32] H.-J. Schmidt, A. Lohmann, and J. Richter, *Phys. Rev. B* **84**, 104443 (2011).
- [33] M. E. Zhitomirsky and T. Nikuni, *Phys. Rev. B* **57**, 5013 (1998).
- [34] M. Bouvier, P. Lethuillier, and D. Schmitt, *Phys. Rev. B* **43**, 13137 (1991).
- [35] S. Nakatsuji, Y. Nambu, H. Tonomura, O. Sakai, S. Jonas, C. Broholm, H. Tsunetsugu, Y. Qiu, and Y. Maeno, *Science* **309**, 1697 (2005).
- [36] Y. Okamoto, M. Nohara, H. Aruga-Katori, and H. Takagi, *Phys. Rev. Lett.* **99**, 137207 (2007).
- [37] J. G. Cheng, G. Li, L. Balicas, J. S. Zhou, J. B. Goodenough, C. Xu, and H. D. Zhou, *Phys. Rev. Lett.* **107**, 197204 (2011).
- [38] A. Yaouanc and P. Dalmas de Rotier, *Muon Spin Rotation, Relaxation, and Resonance: Applications to Condensed Matter* (Oxford University Press, Oxford, 2011).
- [39] Y. J. Uemura, A. Keren, K. Kojima, L. P. Le, G. M. Luke, W. D. Wu, Y. Ajiro, T. Asano, Y. Kuriyama, M. Mekata, H. Kikuchi, and K. Kakurai, *Phys. Rev. Lett.* **73**, 3306 (1994).
- [40] K. Kojima, A. Keren, L. P. Le, G. M. Luke, B. Nachumi, W. D. Wu, Y. J. Uemura, K. Kiyono, S. Miyasaka, H. Takagi, and S. Uchida, *Phys. Rev. Lett.* **74**, 3471 (1995).
- [41] W.-J. Lee, S.-H. Do, S. Yoon, S. Lee, Y. S. Choi, D. J. Jang, M. Brando, M. Lee, E. S. Choi, S. Ji, Z. H. Jang, B. J. Suh, and K.-Y. Choi, *Phys. Rev. B* **96**, 014432 (2017).
- [42] J. S. Gardner, S. R. Dunsiger, B. D. Gaulin, M. J. P. Gingras, J. E. Greedan, R. F. Kiefl, M. D. Lumsden, W. A. MacFarlane, N. P. Raju, J. E. Sonier, I. Swainson, and Z. Tun, *Phys. Rev. Lett.* **82**, 1012 (1999).
- [43] P. Mendels, F. Bert, M. A. de Vries, A. Olariu, A. Harrison, F. Duc, J. C. Trombe, J. S. Lord, A. Amato, and C. Baines, *Phys. Rev. Lett.* **98**, 077204 (2007).
- [44] A. Yaouanc, P. Dalmas de Reotier, A. Bertin, C. Marin, E. Lhotel, A. Amato, and C. Baines, *Phys. Rev. B* **91**, 104427 (2015).
- [45] C. Balz, B. Lake, J. Reuther, H. Luetkens, R. Schönemann, T. Herrmannsdörfer, Y. Singh, A. T. M. Nazmul Islam, E. M. Wheeler, J. A. Rodriguez-Rivera, T. Guidi, G. G. Simeoni, C. Baines, and H. Ryll, *Nat. Phys.* **12**, 942 (2016).
- [46] Y. Li, D. Adroja, P. K. Biswas, P. J. Baker, Q. Zhang, J. Liu, A. A. Tsirlin, P. Gegenwart, and Q. Zhang, *Phys. Rev. Lett.* **117**, 097201 (2016).
- [47] J. A. Quilliam, F. Bert, A. Manseau, C. Darie, C. Guillot-Deudon, C. Payen, C. Baines, A. Amato, and P. Mendels, *Phys. Rev. B* **93**, 214432 (2016).
- [48] Y. S. Choi, C. H. Lee, S. Lee, S. Yoon, W.-J. Lee, J. Park, A. Ali, Y. Singh, J.-C. Orain, G. Kim, J.-S. Rhyee, W.-T. Chen, F. C. Chou, and K.-Y. Choi, *Phys. Rev. Lett.* **122**, 167202 (2019).
- [49] R. Sarkar, Ph. Schlender, V. Grinenko, E. Haeussler, P. J. Baker, Th. Doert, and H.-H. Klauss, *Phys. Rev. B* **100**, 241116(R) (2019).
- [50] A. Keren and G. Bazalitsky, *Physica B* **289-290**, 205 (2000).
- [51] A. Keren, G. Bazalitsky, I. Campbell, and J. S. Lord, *Phys. Rev. B* **64**, 054403 (2001).
- [52] W. Hong, L. Liu, C. Liu, X. Ma, A. Koda, X. Li, J. Song, W. Yang, J. Yang, P. Cheng, H. Zhang, W. Bao, X. Ma, D. Chen, K. Sun, W. Guo, H. Luo, A. W. Sandvik, and S. Li, *Phys. Rev. Lett.* **126**, 037201 (2021).